Reconfigurable optical interconnection network for multimode optical fiber sensor arrays

R. T. Chen, MEMBER SPIE
D. Robinson
H. Lu, MEMBER SPIE
M. R. Wang, MEMBER SPIE
T. Jannson, MEMBER SPIE
Physical Optics Corporation
2545 West 237th Street, Suite B
Torrance, California 90505

R. Baumbick
NASA Lewis Research Center
MS 77-1, Building 28
21000 Brookpark Road
Cleveland, Ohio 44135-3127

Abstract. A single-source, single-detector architecture has been developed to implement a reconfigurable optical interconnection network for multimode optical fiber sensor arrays. The network was realized by integrating $LiNbO_3$ electro-optic (EO) gratings working at the Raman Nath regime and a massive fan-out waveguide hologram (WH) working at the Bragg regime onto a multimode glass waveguide. The glass waveguide utilized the whole substrate as a guiding medium. A 1-to-59 massive waveguide fan-out was demonstrated using a WH operating at 514 nm. Measured diffraction efficiency of 59% was experimentally confirmed. Reconfigurability of the interconnection was carried out by generating an EO grating through an externally applied electric field. Unlike conventional single-mode integrated optical devices, the guided mode demonstrated here has an azimuthal symmetry in mode profile which is the same as that of a fiber mode.

Subject terms: optical interconnections; multimode fiber sensor arrays.

Optical Engineering 31(5), 1098-1106 (May 1992).

1 Introduction

Optical fiber arrays have been proposed for signal paths in various civilian and military controls as a means of offering advanced sensing functions not available in electronic systems, reducing the weight of a control system, and eliminating electromagnetic interference (EMI). Optical fiber data transmission lines and a myriad of sensors have been developed[1-4] for such applications. To implement optic fiber sensors on various control systems, a proper electro-optic architecture (EOA) needs to be studied. Among the many EOAs that have been investigated[5] [such as multiple sources and multiple detector (MSMD) topology, single source and multiple detector (SSMD) topology, multiple sources and single detector (MSSD) topology, and single source and single detector (SSSD) topology], SSSD topology seems to be the most promising. Figure 1 shows a feasible electro-optic architecture for this application. The number of light sources and detectors are minimized in this case; however, to realize such an EOA, proper electro-optic switching elements are needed to multiplex (receive) and demultiplex (transmit) optical carriers in the time domain so that the specific direction where proper fiber sensors or receivers are located can be selected. To date, most integrated optic switches are not compatible with multimode fibers[6-8] when employing data or for short distance communication, i.e., within a ship or an airplane. Therefore, there exists a need to develop a new electro-optic switch to overcome the above shortages.

Paper 2442 received Dec. 26, 1990; revised manuscript received Oct. 15, 1991; accepted for publication Oct. 15, 1991.

Optical fiber sensing devices have so many advantages over other types of sensing devices that they have become the focus of a significant amount of research. Physical parameters such as position, velocity, acceleration, temperature, pressure, vibration, voltage, and current, can be successfully measured via fiber optic sensor technology. The multimode switching system we built in this program encompasses all these scenarios of fiber sensor technologies. Since the communication distance from the sensors to the processing unit is relatively short (< 100 m), multimode fiber is selected to route the sensed signals.

The major bottleneck for the implementation of multimode fiber sensor arrays is the mismatch between existing electro-optic switching devices and multiple mode fiber. This issue becomes more difficult when the power budget is strictly limited. The existing multimode optical switches fall into two categories: moving fiber and scanning optical beam. There are three fundamental problems that preclude their use in high-speed multiplexer systems for the reconfigurable massive fan-out sensor systems:

1. *Low fan out/fan in capability.* The moving fiber and scanning technologies basically provide 1-to-1 interconnection. Beam scanning provided by an acoustic Bragg cell can provide hundreds of resolvable spots. However, such a device can only provide reconfigurable 1-to-1 interconnection. The usefulness of the AO scanner depends on the electro-optic architecture and the number of sensors to be used. In the case of a small interconnection system where the number of sensors involved is relatively small, the A-O scanner may be a proper candidate.

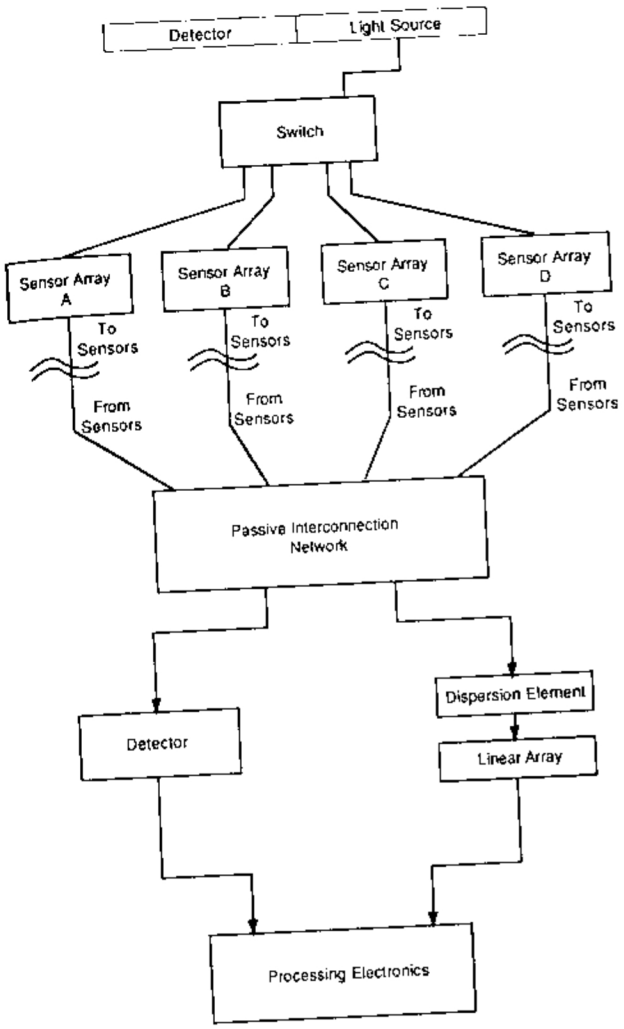

Fig. 1 Electro-optic architecture for multimode fiber sensor array.

2. *High insertion loss.* The losses associated with the moving fiber and scanner are high, which makes the system insertion loss unacceptable. This kind of loss is mainly induced by beam divergence, Fresnel reflection, scattering and mode mismatch.
3. *Slow switching speed.* Moving fibers involve the adjustment of mechanical parts and the speed is intrinsically slow. Scanner devices, except the A-O Bragg cell, have the same problems as moving fibers. Fast switching speed is important for fast access of the sensor signal.

Due to the aforementioned problems of existing multimode switches, new switching elements are needed to fulfill the requirements of large fiber sensor array systems.

In this paper, we developed a new type of electro-optic switch that provides vertical coupling geometry, massive fan-out/fan-in capability, low insertion loss and high switching speed and compatibility with multimode fiber. An electro-optic switching array proposed to meet the requirements of the electro-optic architecture (Fig. 1) is presented. The whole system is built on a glass waveguide which relays the optical signal from light sources such as laser diodes and LEDs to fiber sensor arrays. The selection of the optical wave from light sources to a specific sensor or sensor array is controlled by the cascaded multimode electro-optic switching elements. Note that the glass waveguide defined herein utilizes the whole substrate as the guiding medium. The mode distribution has a continuous mode spectrum, which is usually defined as the substrate mode in integrated optics.

2 Electro-Optic Switching Device for Multimode Fiber Sensor Array

Integrated electro-optic modulators have been studied for more than two decades. Electro-optic modulation of light can be separated into phase, polarization, and intensity modulation. One of the most popular types is the directional coupler.[9–11] Because of the overlap in the evanescent fields of two waveguides, light couples between them with a coupling coefficient depending on the waveguide parameters, wavelength, and interwaveguide separation. With the proper conditions, all of the light entering one waveguide can couple to the other. By electro-optically producing an index difference between the two waveguides, light that crosses over at different points along the directional coupler is no longer in phase and the net cross-over efficiency can be made zero. Another modulation scheme is the integrated optic version of the Mach–Zehnder interferometer[12,13] with one input channel and one output channel. It was first reported by Martin in 1975.[12] This type of modulator employs the interference of coherent light going through different lengths of optical path which can be controlled by external bias. The throughput intensity will be modulated due to the phase difference. Four other promising waveguide modulators are the cutoff,[14] phase,[15] total internal reflection (TIR),[16] and X switches.[17]

Each of the above intensity modulators has been demonstrated on insulating and semiconductor substrates. All of them employ thin film dielectric waveguides as the fundamental building blocks with a combination of properly designed electrode patterns. A high-frequency, wide bandwidth electro-optic modulator of up to 20 GHz at 1.3 μm has been achieved.[18] A modulator array with 500 channels/cm packing density on GaAs–GaAlAs heterostructure has also been published.[19]

The existing switching devices in integrated optics are compatible only with single-mode fiber. Integrated optic switching devices are intrinsically not compatible with multimode fiber due to the different mode profiles and guiding layer geometries between multimode fiber and single-mode waveguides.

To solve the interface problems, we developed a novel electro-optic grating switch architecture that is capable of matching well with multimode fiber. Phase gratings can be directly induced in electro-optic materials through the use of interdigitated electrodes on the surface of the electro-optic material. The EO grating working in the single-mode scenario is well known in integrated optics. The concept of the presented architecture (Fig. 2) is that it implements an active device on a thin low-index plate, typically 10 to 100 mils. The plate is used as the guiding medium to route optical waves from light sources to the desired locations where fiber sensors are located. A comparison of the conventional integrated-optic grating switch and the newly proposed EO grating is shown in Fig. 3. Figure 3(a) shows the traditional

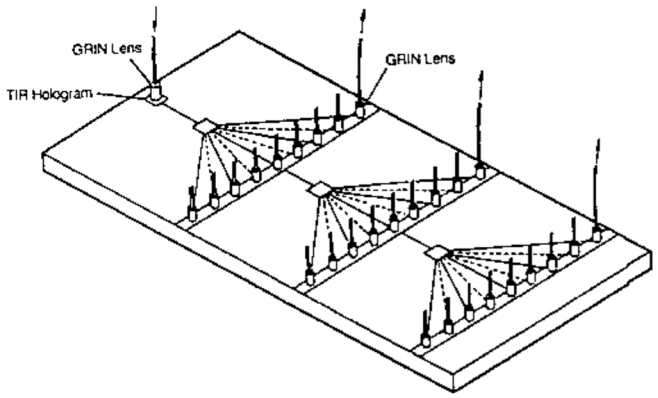

Fig. 2 Cascaded switching array using Raman–Nath electro-optic gratings.

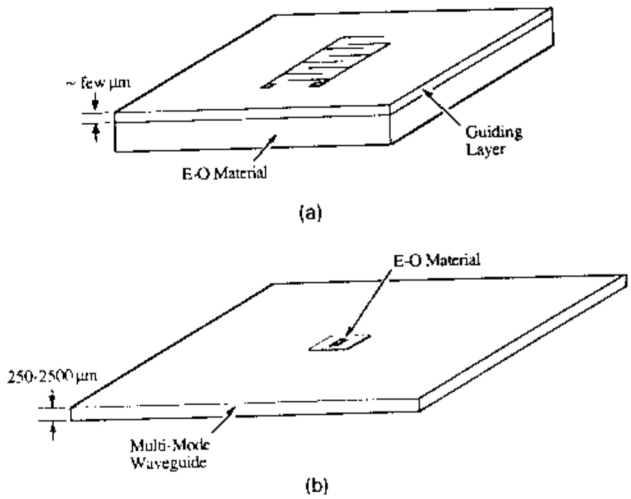

Fig. 3 EO gratings in (a) traditional single-mode integrated optics and (b) newly developed device structure.

integrated optic electro-optic grating switch. The guiding medium is typically from submicrometers to a few micrometers. Typical multimode fiber has a core diameter of 100 μm and it is obvious that compatibility between these two devices is not possible. The proposed EO switch is shown in Fig. 3(b). The output beam profiles of this device and multimode fiber are extremely well matched. The result will be demonstrated in Sec. 4.

2.1 *Theory of Operation*

Beam diffraction, as a mechanism for intensity modulation by electro-optic means in thin films, is achieved by producing an electrically controlled phase grating in the path of the propagating beam. The diffraction process results from a periodic perturbation of the refractive index transverse to the beam propagation direction. A useful method for electro-optically generating the desired phase grating is shown in Fig. 4. The mechanism for interaction relies on the fringes of electric fields extending below the surface between interdigital strip electrodes formed on the EO crystal surface. The local fringing field strength should be reasonably uniform across the guided beam and periodically perturbed in the plane of the guiding layer, transverse to the beam.

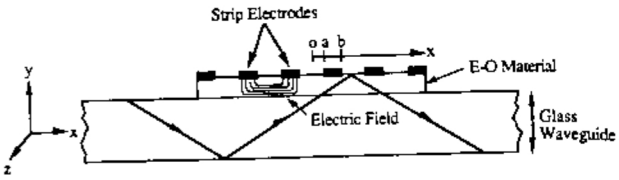

Fig. 4 Phase grating formation by electro-optic effect.

Bragg diffraction involves introducing the input beam at a specific angle θ_B, the Bragg angle, with respect to the electrode array.[20,21] Diffraction occurs reflectively in a single output at twice the input angle when the Bragg condition is satisfied.

The phase change ϕ, in radians, induced by the electrical signal field over a pathlength L is

$$\phi = [(2\pi L)/\lambda_0]\Delta n \ , \tag{1}$$

where Δn is the refractive index increment caused by the electro-optic effect and λ_0 is the free-space wavelength. The strongest interaction in uniaxial crystals, such as $LiTaO_3$ and $LiNbO_3$, occurs when the applied electric field and optical electric polarization are both parallel, or nearly parallel, to the crystalline c axis (optic axis). For this condition, the refractive-index increment is

$$\Delta n_3 = \frac{1}{2} n_e^3 r_{33} E_3 \ , \tag{2}$$

where n_e is the extraordinary refractive index, r_{33} is the appropriate electro-optic coefficient, and E_3 is the applied electric field. Thus, the crystal must be cut with its c axis in the plane of the waveguide essentially transverse to the incident beam propagation direction, and the propagating optical mode must have TE (transverse electric) polarization. This polarization has the least loss characteristics in proximity to the metal electrode surfaces. Thus, this minimizes the insertion loss of the modulator which was caused by absorption. Combining Eqs. (1) and (2) yields

$$\phi = \frac{\pi L n_3^3 r_{33} E_3}{\lambda_0} \ . \tag{3}$$

Assume that the c-axis-oriented electric field in the region of the guided layer is approximately sinusoidal in the transverse direction. For Bragg diffraction, the zero- and first-order powers are proportional, respectively, to $\cos^2(\phi/2)$ and $\sin^2(\phi/2)$. For modulation, corresponding to 100% depletion of the zero-order beam in the idealized case, the maximum required value of ϕ is π.

In our device, the optical wave bounces up and down, as shown in Fig. 4. The interaction length l_ℓ, i.e., the length over which index modulation exists, is

$$l_\ell < 2d/\cos\theta \tag{4}$$

where d is the thickness of the electro-optic material, which is 0.5 mm in our demonstration, and θ is the bouncing angle. The upper limit exists because the glass waveguide has no linear electro-optic property. To evaluate the interaction length we need to first compute the electric field distribution, which is related to index modulation by Eq. (2).

The electrode configuration for which the change in refractive index will be computed is shown in Fig. 4. The electric field $E_x(y)$ along the y axis is given by[20,21]

$$E_x = \frac{-U}{2K} \frac{a}{[(a^2+y'^2)(a^2+k^2y'^2)]^{1/2}} , \tag{5}$$

where $y' = (n_x/n_y)y$, $k = a/b$, and K is the complete elliptical integral of the first kind.[21] An important conclusion of this calculation is that the effective interaction length L_{eff}, which is defined as the distance above which Δn_x is less than e^{-1} of the surface index modulation, is in the range of 150 to 450 μm.[21] Exact L_{eff} is a function of the ratio of a/b.

2.2 *Switching Speed*

An important parameter for the electrode configuration is the distributed capacitance C.[22] This capacitance, together with the load resistor R, determines the base bandwidth Δf of the modulator, which is correlated with switching speed T by

$$T = \frac{2\pi}{\Delta f} \tag{6}$$

when driven by a matched source

$$\Delta f = (\pi RC)^{-1} . \tag{7}$$

In the previous section, we calculated the interaction length of interdigital electrodes. The interdigitated electrode structure of a grating modulator, the net capacitance per unit length per gap between electrodes, is[23]

$$C = \varepsilon_{\text{eff}}/2V_0 , \tag{8}$$

where ε_{eff} is the effective permittivity. Minimizing the switching time is most important when large-scale arrays or switches and modulators are used to route optical waves over desired paths. Similarly, modulation bandwidth is a critical factor when many information channels are to be multiplexed onto the same optical beam. Thus, the usually fast switching speed and large bandwidths of waveguide switches and modulators make them particularly useful in large and highly parallel communications systems. The capacitance of the planar electrodes was calculated using the conformal mapping method. With $R = 50\ \Omega$, a 130-MHz modulation bandwidth results, which corresponds to ~50-ns switching time ($T = 2\pi/\Delta f$). The speed is much faster than that of moving fibers and scanning devices. The electro-optic grating used has 80 fingers. Further increase of switching speed can be successfully achieved by reducing the number of fingers. A switching network compatible with FDDI standards is achievable.

The maximum number of interconnection channels depends upon the power budget of each sensor system. The elements of the optical power budget are the source power intensity, the insertion losses of the interconnection network, and the signal-to-noise ratio required to obtain the desired level of sensor performance/sensitivity. For fiber optic sensors, a wide dynamic range receiver is usually required, so a PIN photodiode with a transimpedance-type preamplifier is the receiver design of choice. For digital sensors, the signal-to-noise ratio must be at least 12 to achieve a bit error rate better than 10^{-9}.

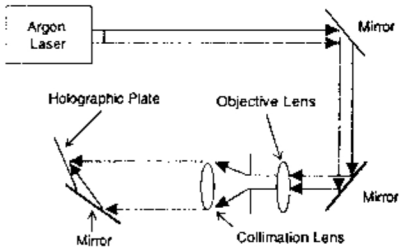

Fig. 5 Experimental setup for waveguide hologram formation.

These data actually determine the minimum power level needed at the receiver end. The combination of these data with other loss factors such as coupling and propagation loss determines the minimum input power required for each spot.

3 Hologram Fabrication

To efficiently couple optical waves from fiber to waveguide and then from waveguide to fiber, a volume hologram, i.e., with emulsion thickness much larger than optical wavelength, needs to be created.

3.1 *Formation of High-Efficiency TIR Hologram*

To construct a high-efficiency TIR hologram that couples free space TEM_{00} light into a multimode glass waveguide, the setup shown in Fig. 5 is required. Depending on the absorption bandwidth of the holographic emulsion, a proper recording wavelength can be chosen. Various types of transmission holograms can be constructed by using this setup configuration. The grating spacing is given by

$$\Lambda = \frac{\lambda}{2n_r \sin\theta} \tag{9}$$

in an unslanted case. In Eq. (9), λ is the recording wavelength, θ is the half angle between the two recording beams, and n_r is the refractive index of the medium on top of the holographic emulsion. For optical interconnection of the planar geometry, the grating vector **K**, which is defined as $2\pi/\Lambda$, shall be in the same plane as the incident and deflected guided optical beams. In the case of three-dimensional coupling, such as free space to waveguide, the Bragg plane of the grating may be slanted to increase the coupling efficiency. To form a slanted grating coupler that converts a vertical incident wave to a total internal reflection mode with bouncing angle α, the two incident angles of the recording beams are

$$\theta_1 = \sin^{-1}[n/n_r(\sin\delta)] , \tag{10}$$

$$\theta_2 = \sin^{-1}\{n/n_r[\sin(\alpha-\delta)]\} , \tag{11}$$

where n is the index of refraction of the hologram and n_r is the refractive index of the medium on top of the DCG hologram ($n_r = 1$ for air) and

$$\delta = \frac{\alpha}{2} - \sin^{-1}\left\{\frac{\lambda_b}{\lambda_r}\left[\sin\left(\frac{\alpha}{2}\right)\right]\right\} \tag{12}$$

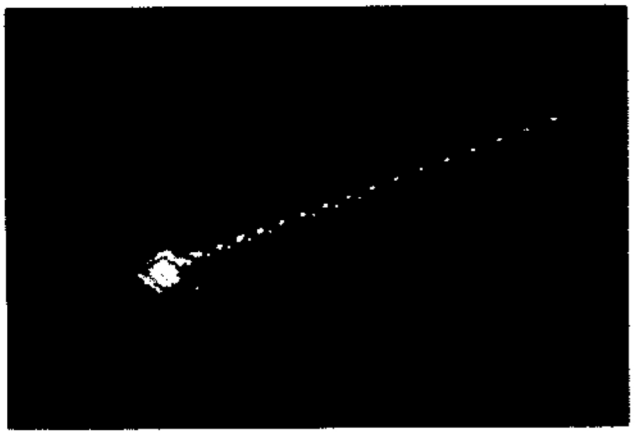

Fig. 6 Waveguide coupling using TIR hologram.

In Eq. (12) λ_b and λ_r represent the wavelengths of recording and reconstructing waves, respectively.

To increase angle α, i.e., to increase the bouncing distance, one can either decrease the ratio of λ_b/λ_r by changing the recording and reconstructing wavelengths or increase n_r by putting a high index prism directly on top of the holographic plate. Coupling of laser light into a 250-μm glass waveguide with a high-efficiency TIR hologram as the input coupler is shown in Fig. 6. The hologram was recorded at 457 nm (argon laser) and reconstructed at 632.8 nm. To provide laser to waveguide coupling with a wider bandwidth, cascaded TIR holograms with different center frequencies can be combined together. Figure 6 shows the free space to waveguide coupling through a TIR hologram working at 632.8 nm. A bright streak is clearly observed.

3.2 *Formation of Massive Fan-out Hologram*

To construct an intraplane massive fan-out interconnection network, a multiplexed waveguide hologram is needed. Unlike the TIR hologram introduced in the previous section, the hologram constructed is to provide a 1-to-many fan-out. Each fan-out beam goes to an optical fiber corresponding to an optical sensor shown in Fig. 2. Note that the continuous spectrum of the guided mode wavevector significantly eases the requirement for the grating vector. For each fan-out direction, a proper recording geometry is designed to introduce reference and object beams with precise incident directions. A 1-to-59 waveguide fan-out hologram working at 514 nm was fabricated. The fan-out beams are shown in Fig. 7(a). The 59 mode dots were coupled out of a prism coupler. The measured diffraction efficiency of each individual fan-out beam is illustrated in Fig. 7(b). The angle of the fan-out beams varies from 10 to 69 deg. Total diffraction efficiency of 59% was experimentally confirmed.

4 Experimental Results

In Fig. 2, the cascaded fiber arrays are situated so that various diffraction orders can be successfully coupled into preselected fibers. The electro-optic grating was designed so that

$$\mathbf{K}_{out} = \mathbf{K}_{in} + n\mathbf{K} \qquad n = 0, \pm 1, \pm 2, \ldots , \tag{13}$$

where $\mathbf{K}_{out}$ and $\mathbf{K}_{in}$ are defined as

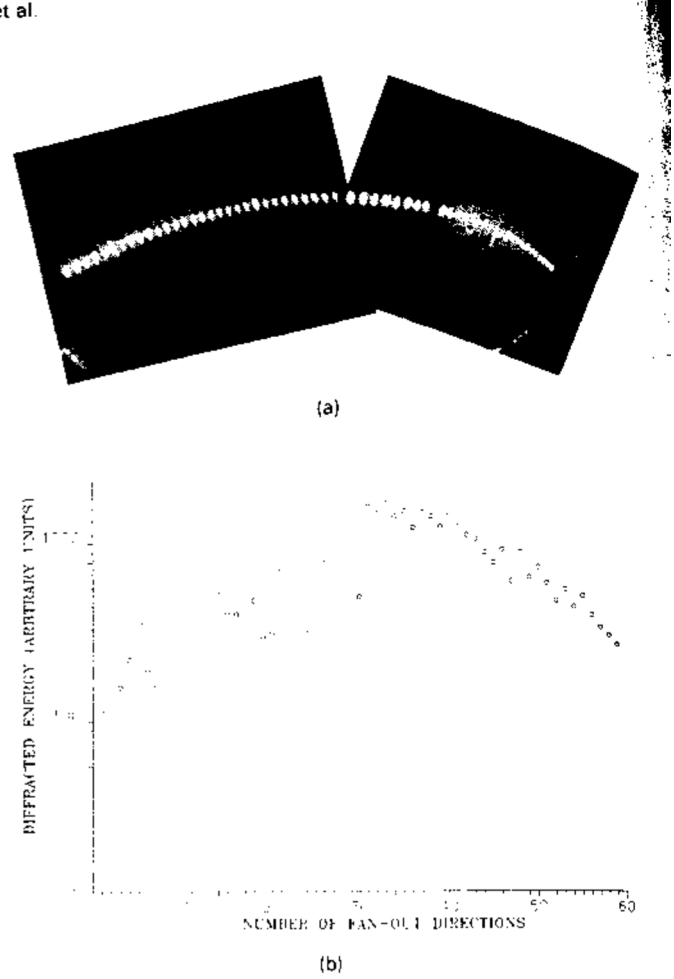

Fig. 7 (a) A 1-to-59 waveguide fan-out hologram working at 514 nm, 59 mode dots coupled out of a prism coupler. (b) Measured diffracted energy of each individual fan-out beam.

$$\mathbf{K}_{out} = \mathbf{K}_{in} = \frac{2\pi}{\lambda} \tag{14}$$

and $\mathbf{K}$ is the electro-optic grating vector. The electro-optic grating we employed for this application has a grating spacing of $\Lambda = 40$ μm. Many diffraction orders have been observed. Note that the waveguide structure we used in the application is not the conventional type with waveguide dimension close to diffraction limitation (submicrometer to a few micrometers). The waveguide mode we defined is sometimes called a substrate mode in integrated optics. We define this type of device as a multimode waveguide for two reasons: (1) the optical wave is guided and propagated in a well-defined direction and (2) all optical waves that satisfy total internal reflection conditions can be guided modes defined herein. One of the most important results in employing this type of waveguide is that the insertion loss for coupling between waveguide and multimode fiber is extremely low (< -0.5 dB/joint). Furthermore, the waveguide propagation loss was measured to be less than 0.1 dB/cm, which significantly reduces the system power budget requirement. The mode profile of this multimode waveguide, which used thin glass substrate as the guiding medium, is well matched with the near field pattern of guided modes of multimode fiber. The near field pattern of the guided mode of these two guided wave devices are shown in Fig.

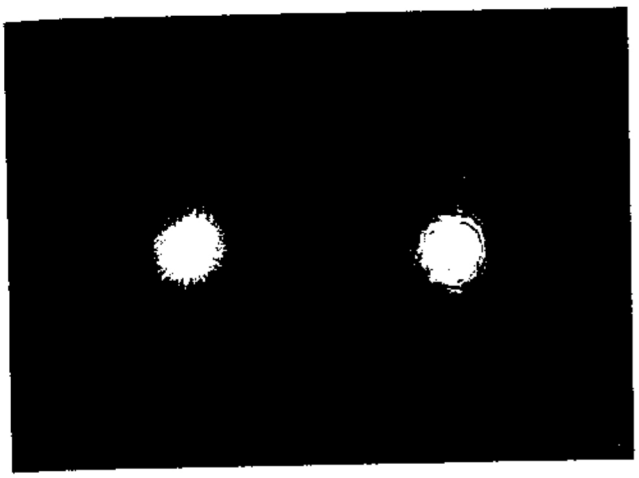

Fig. 8 Near-field patterns of the guided wave of multimode fiber (left) and multimode glass waveguide (right, 100 μm in diameter).

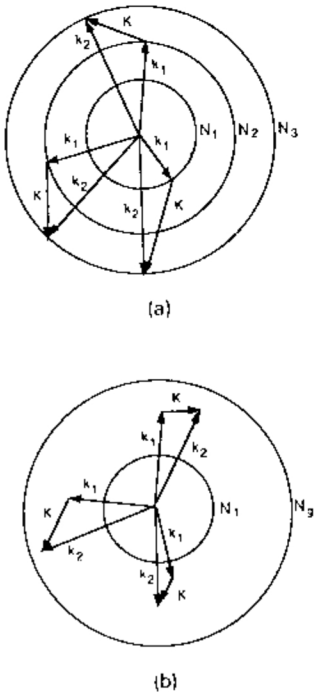

Fig. 9 Phase-matching conditions for (a) conventional and (b) new waveguide structures.

8. The waveguide mode was coupled out through a TIR hologram.[24] The interface problem we described in the beginning of this paper is therefore solved due to the continuity of the guided mode profiles of these two different devices. The output mode profile is independent of the glass substrate thickness.

The phase matching condition can be easily achieved by manipulating the guided wave propagation direction and bouncing angle. In the case of conventional guided wave devices, to construct a grating vector **K** that can deflect incident guided waves to certain directions, the spatial frequency of such gratings needs to be controlled carefully so that the required phase matching condition can be fulfilled. From this technical point of view, such stringent requirements impose a bottleneck on the coupling angle adjustment. To make this issue clear, Fig. 9 illustrates the difference between these two different waveguide structures.

Figure 9(a) shows a conventional multimode waveguide with three guided modes. To construct a grating to efficiently deflect the incident guided wave in certain directions, the grating vector needs to touch the circumference. In the case of the new multimode waveguide structure we used in the fiber sensor array interconnection network, the phase matching condition required for beam steering can be easily achieved. Any grating vector **K** within the two circumferences, which are the wave numbers corresponding to the total internal reflection value and glass refractive index value, can create the phase-matched diffraction beam shown in Fig. 9(b). This occurs in this case because the spectrum of the effective indices of guided modes is continuous rather than quantized.

Demonstration of the whole package including input multimode fiber, GRIN lens, TIR input hologram, glass waveguide, $LiNbO_3$ electro-optic grating, and TIR output coupler is shown in Fig. 10. The index of refraction of lithium niobate is higher than that of glass and, therefore, the guided mode in the glass substrate penetrated through the $LiNbO_3$ and interacted with the active region of the EO grating located on the top surface of $LiNbO_3$. The electrode was made of Cr/Al. Accordingly, a diffraction grating existed when there was no external E field added (static grating effect). Use of such a grating can provide an electro-optic power divider for the 1-to-many fiber sensor interconnection. If this type of interconnection is not desired, the electrode should be made of transparent materials such as ITO (indium tin oxide). In this case 1-to-many fan-out is provided only by external voltage. Application of an external voltage generated a refraction index modulation due to the Pockel effect. The grating space used is quite large (40 μm) and it is expected that a few hundred volts were required to switch off the 0'th order light. Figure 11 shows the measured diffraction efficiency of the 0'th order light. The solid line represents the theoretical prediction and the dotted line is the measured experimental results. The far field image of many diffraction orders at $V=0$ and $V=350$ V is shown in Fig. 12(a) and the measured diffraction efficiency of each order is shown in Fig. 12(b). Note that switching voltage in the neighborhood of 10 V can be realized using ferroelectric liquid crystal as the active medium. The existence of diffraction at $V=0$ V is due to the static grating slits generated by the Ar/Al electrode. Figure 12(a) was taken at an image plane perpendicular to the output TIR grating coupler [Fig. 10(b)]. An array of bright spots is clearly observed. Each individual spot corresponds to one output fiber that routes the optical wave to the site where the sensing device is located.

The total number of interconnection points, i.e., the number of fiber sensors involved in the network, will determine the final size of the package. An alternative to provide 1-to-many reconfigurable optical interconnects is to implement a 1-to-1 electro-optic grating functioning in the Bragg regime in conjunction with a highly multiplexed transmission hologram (HMTH) and each HMTH routes optical signals to a specific group of fiber sensors.[21]

(a)

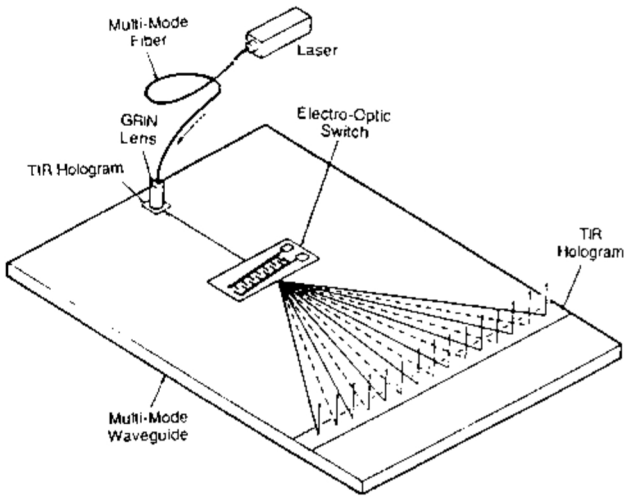

(b)

Fig. 10 (a) Demonstration of multimode switch working at the Raman–Nath regime with vertical couple in and out features. (b) Schematic of (a).

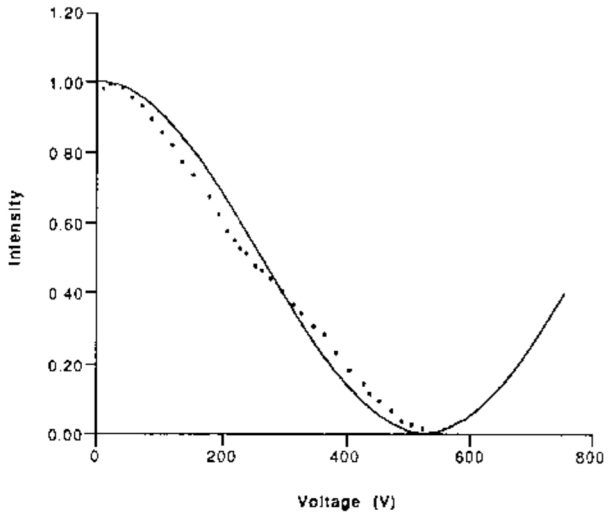

Fig. 11 Measured diffraction efficiency of the 0-th order light.

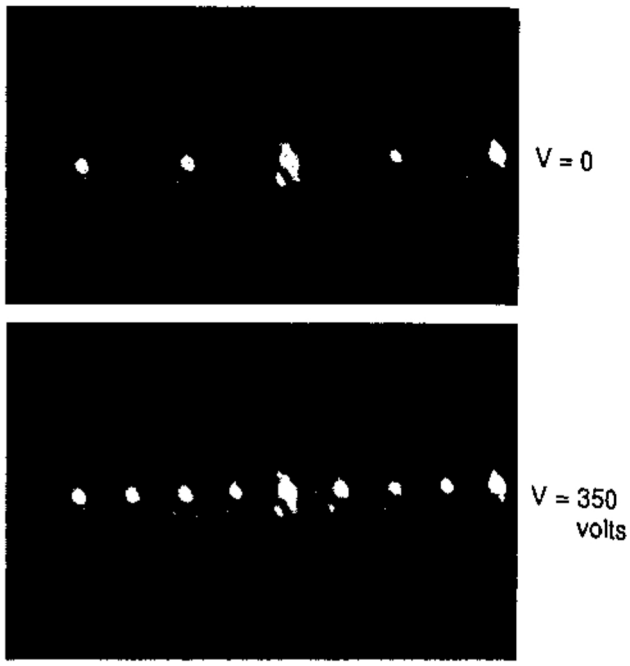

(a)

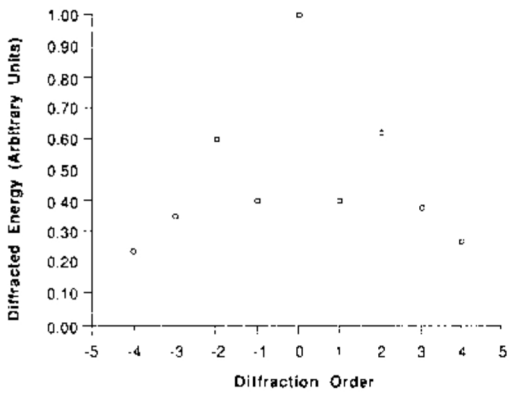

(b)

Fig. 12 (a) Near-field output pattern directly coupled out from the TIR hologram (Fig. 10). (b) Measured diffraction efficiency of different diffraction orders ($V = 350$ V).

5 Further Applications

Many far-reaching applications can be realized based on the proposed technology. Basically, the multimode electro-optic grating switch we proposed and then developed is suitable for all the optical and electro-optic systems that involve optical interconnection among multimode fibers. Some of the more highly plausible applications are further described in this section.

For interconnection distance within the dispersion limit, multimode fiber can be employed to transmit signals. The multiple-mode electro-optic switch we developed can be used as the switching device for the local area network signal distribution. Switching voltage can be significantly reduced by choosing a ferroelectric liquid crystal as the EO material

that has an EO coefficient two orders of magnitude higher than $LiNbO_3$.

The EO switching device we developed herein can also be used as a large dynamic range voltage sensor. The dynamic range of the voltage can be adjusted by the spacing of the interdigitated grating. The light intensity as a function of applied voltages is predictable. The light intensity in the m-th-order diffraction order $I_i(m, V)$ is predicted by[25]

$$I_i(m, V) = I_i(0,0)\frac{\sin^2(m\pi g/2d)}{(m\pi g/2d)^2} \times \cos^2\left(\frac{m\pi}{2}+\frac{\pi V}{2V_{\pi i}}\right) \qquad i=1, 3 , \tag{15}$$

where $i=1, 3$ refers to the incident beam polarization along the x (ordinary index) and z (extraordinary index) axes, g is the clear aperture, d is the electrode center to center spacing, and $V_{\pi i}$ is the voltage required for a relative phase change of one-half wavelength (π radians) between adjacent interelectrode gaps. It is clear from Eq. (15) that higher diffraction orders can also be used to enlarge the range of voltage measurement.

6 Conclusions

In summary, we achieved the first electro-optic grating switch for a multimode optical fiber sensor array. A 1-to-many cascaded reconfigurable interconnection was built based on this technology. A thin glass substrate was used as the guiding medium, which provides not only higher coupling efficiency from multimode fiber to waveguide but also better tolerance of phase matching conditions. Involvement of a TIR hologram and multimode waveguide eliminates interface problems between fibers and waveguides due to the azimuthal symmetry of the guided modes. $LiNbO_3$ was chosen as the EO material because of its stability at high temperatures, and maturity of EO device technology. The electro-optic grating was designed in the Raman–Nath regime to provide a 1-to-many interconnection. The switching voltage can be significantly reduced when ferroelectric liquid crystal is implemented. Fabrication of a TIR hologram and a highly multiplexed waveguide fan-out hologram are reported in this paper. A 1-to-59 massive fan-out was demonstrated at 514 nm with 59% combined diffraction efficiency.

Acknowledgment

This program was sponsored by the joint program office of the National Aerospace plane (NASP) at Wright Patterson AFB and the NASA Lewis Research Center.

References

1. R. O. Stanton, "Digital optical transducers for helicopter flight control systems," *SPIE Proc.* **412,** 122 (1983).
2. J. Farina, R. Hubbard, and P. Lefkowitz, Development and Test of a Digital/Optical Rotary Position Transducer. USSAAVRADCOM TR 83-D-15, U.S. Army Research and Technology Laboratories, Ft. Eustis, VA (1983).
3. D. J. Poumakis and W. J. Davies, Fiber Optic Control System Integration Final Report, Report No. CR 179569 (Dec. 1986).
4. J. C. Russel, "Protocol branch optimization method used in FOCSI program fiber optic control system," *IECE Japan OFS'86 Technical Digest*, 3 (1986).
5. W. L. Glomb Electro-optic Architecture (EOA) for Sensors and Actuators in Aircraft Propulsion Systems, Final Report, NASA Contract NAS3-25343 (1989).
6. K. Ishida, H. Nakamura, R. Matsumura, T. Kadoi, and H. Inoue, "InGaAsP/InP optical switches using carrier induced refractive index change," *Appl. Phys. Lett.* **50,** 141 (1987).
7. S. Tonchev and I. Savatinova, "Optical multimode X-switch in Ti-diffused $LiNbO_3$," *J. Opt. Commun.* **6,** 3 (1985).
8. J. P. Lorenzo and R. A. Soref, "1.3 mm electro-optic silicon switch," *Appl. Phys. Lett.* **51,** 6 (1987).
9. M. Papuchon, "Electrically switched optical directional coupler: Cobra," *Appl. Phys. Lett.* **27,** 289 (1975).
10. R. T. Chen, L. Sadovnik, T. Jannson, and J. Jannson, "Single-mode polymer waveguide modulator," *Appl. Phys. Lett.* **58,** 1 (1991).
11. R. C. Alferness, R. V. Schmidt, and E. H. Turner, "Characterization of Ti-diffused $LiNbO_3$ optical directional coupler," *Appl. Opt.* **18,** 4012 (1979).
12. W. E. Martin, "A new waveguide switch/modulator for integrated optics," *Appl. Phys. Lett.* **32,** 562 (1975).
13. V. Ramaswamy, M. D. Divino, and R. D. Standley, "Balanced bridge modulator switch using Ti-diffused $LiNbO_3$ strip waveguides," *Appl. Phys. Lett.* **32,** 644–646 (1978).
14. R. T. Chen and C. S. Tsai, "Thermally annealed single-mode proton-exchanged channel waveguide cut off modulator," *Opt. Lett.* **11,** 546 (1986).
15. C. L. Chang and C. S. Tsai, "Electro-optic analog-to-digital convertor using channel waveguide Fabry–Perot modulator array," *Appl. Phys. Lett.* **43,** 22 (1983).
16. C. S. Tsai, B. Kim, and F. R. El-Akkari, "Optical channel waveguide switch and coupler using total internal reflection," *IEEE J. Quantum Electron* **QE-14,** 539 (1978).
17. A. Neyer, "Electro-optic X-switching using single-mode Ti:$LiNbO_3$ channel waveguides," *Electron. Lett.* **19,** 553 (1983).
18. S. Y. Wang, S. H. Lin, and M. Huong, "GaAs traveling-wave polarization electro-optic waveguide modulator with bandwidth in excess of 20 GHz at 1.3 μm, *Appl. Phys. Lett.* **51,** 83 (1987).
19. R. T. Chen and C. S. Tsai, "GaAs–GaAlAs heterostructure single-mode channel waveguide cutoff modulator and modulator array," *IEEE J. Quantum Electron.* **QE-23,** 2205 (1987).
20. P. Moon and D. E. Spencer, *Field Theory Handbook*, Springer, Berlin (1961).
21. P. Vandenbalcke and P. E. Lagasse, "Static field analysis of thin film electro-optic light modulator and switches," *Wave Electron.* **1,** 295 (1974); E. Durand, *Electorstatique*, Masson, Paris (1966); and R. T. Chen, "Multiple-mode optical switching array for fiber optic network," Final Report to WPAFB Contract F33657-89-C-2200 (1990).
22. E. Yamashita and K. A. Atsuki, "Distributed capacitance of a thin electro-optic light modulator," *IEEE Trans. Microwave Theory Tech.* **MTT-23,** 177 (1977).
23. J. S. Wei, "Distributed capacitance of planar electrodes in optic and acoustic surface wave devices," *IEEE J. Quantum Electron.* **QE-13,** 152 (1977).
24. R. T. Chen, M. R. Wang, F. Lin, and T. Jannson, "Thick phase hologram for optical clock distribution application on wafer scale integrated circuits," *Proc. SPIE* **1213,** 27 (1990).
25. R. P. Bocker, "A large-aperture electro-optic diffraction modulator," *J. Appl. Phys.* **50,** 6691 (1979).

Ray T. Chen received his PhD degree in electrical engineering from the University of California, Irvine, under the direction of Prof. Chen S. Tsai. He received his MS and BS degrees in physics from the University of California, San Diego, and National Tsing Hua University, Taiwan, respectively. He is currently the director of the Electro-optic Engineering Department at the Physical Optics Corporation. He has been the author and the principal investigator of 20 awarded research proposals sponsored by many subdivisions of DOD, NSF, DOE, NASA, and private industries. His research topics involve 2-D and 3-D optical interconnects, integrated optics, electro-optic switches/modulators, GaAs all-optical crossbars, $X^{(2)}$ nonlinear polymers, polymer waveguides and waveguide modulators, optical fiber sensors, switching networks for fiber sensor arrays, image processing, holographic lithography and holographic optical elements. Together with a UCLA research team, he has recently demonstrated a board-to-board optical interconnect with 60 GHz bandwidth. He has been the chair as well as a committee member for various SPIE and IEEE conferences. Dr. Chen has more than 60 publications in open literature. He is a member of SPIE, IEEE/LEOS, PSC, and OSA.

Daniel P. Robinson is a research technician with Physical Optics Corporation's Intergrated Optics Group, where he has been working for the past two years. He participated in the research, fabrication, and testing of massive fanout holograms for reconfigurable optical interconnect networks. Prior to his current employment Robinson worked at the NASA Ames-Dryden Flight Loads Research Facility at Edwards Air Force Base. He has completed an electro-optics program at Pasadena City College and is now completing an optics program at the University of La Verne, Calif.

Huey T. Lu has been a research assistant at Physical Optics Corporation since 1989. He is currently responsible for research of microstructure polymer waveguides, optical interconnections, a multichannel wavelength division demultiplexer in the near infrared, and holographic optical switching elements. Prior to joining the Physical Optics Corporation, Lu worked on semiconductor laser characterization and packaging at Plesscor Optronics Inc. Huey is also a student at the University of La Verne, Calif., pursuing his BS in optical engineering. He is a member of SPIE.

M. R. Wang: Biography and photograph not available.

T. Jannson: Biography and photograph not available.

Robert Baumbick: Biography and photograph not available.